Electronic Supplementary Material (ESI) for Inorganic Chemistry Frontiers.

Supplementary Information

Solvent Switching Smart Metal-Organic Framework as catalyst of Reduction and Condensation

Farzaneh Rouhani, Behnam Gharib, Ali Morsali*

Contents

Supplementary Information

Section A. Materials, methods

A.1 All starting materials were purchased from Merck and Aldrich companies and were utilized without further purification. Thermogravimetric analysis (TGA) of the three compounds were studied by computer-controlled PL-STA 1500 apparatus from 25 to 600 ^{o}C into alumina pans with the gradient of 10 ^{o}C/ min under inert atmosphere of N_2. The melting point was measured on an Electrothermal 9100 apparatus and is uncorrected. The IR spectra (in KBr) have been recorded in the range of 4000-400 cm^{-1} by Nicolet Fourier Transform IR, Nicolet 100 spectrometer. The crystallographic measurements of TMU-60 were done by the Bruker APEX area-detector diffractometer. The intensity data were collected using graphite monochromated Mo–Kα radiation (λ=0.71073 Å) at room temperature. The X-ray powder diffraction (XRD) measurements were carried out by using a Philips X'pert diffractometer with monochromated Cu-kα radiation (λ=1.54056A). The N_2 adsorption/desorption isotherm was measured at liquid nitrogen temperature (77 K) using a Micromeritics ASAP 2020 analyzer. The specific surface area was computed by the Brunauer-Emmett-Teller (BET) method. Gas chromatography (GC) runs were performed on an Echrom Gc A90 gas chromatograph.

A.2 Synthesis of N1, N2-bis(pyridin-4-ylmethylene) ethane- 1,2-diamine (L)

Compound L was synthesized by a literature method.[1] 1, 2-Ethylenediamine (1eq) and 4-pyridinecarboxaldehyde (2eq) were mixed in 10 mg of EtOH and refluxed for 4 h; subsequent evaporation of the solvent gave a pale yellow powder of L, which was washed with cold ethanol and dried in air. Mp: 688C, Yield: 80 % (based on amine moiety). IR (KBr, cm^{-1}): 3037(m),2843(s), 1652(m), 1591(s), 1408(m), 1318(w), 1224(w), 1011(w), 813(s), 635(m), 530(m). 1H NMR (500 MHz, DMSO): d 8.6(d, 4 H, ArH), 8.3(s. 2 H, HC=N), 7.61(d,4 H, Ar-H) and 3.9(s, 4 H, HC-C).

Section C. Supplementary spectra (Figure S1-S15)

Table S.1. Selected bond lengths (Å) and angles (º) for TMU-60.

Bond		Angle	
Zn_1-O_3	2.046(2)	**C_{17}-C_{19}-C_{20}**	122.34
Zn_1-N_1	2.026(2)	**C_{19}-C_{20}-C_{20}**	124.80
C_{20}-C_{20}	1.371(3)	**C_{20}-C_{20}-N_2**	120.65
C_{20}-N_2	1.391(3)	**C_{20}-N_2-C_{21}**	116.34
C_{21}-N_2	1.438(4)	**N_2-C_{21}-C_{21}**	110.70
C_{21}-C_{21}	1.496(8)	**C_7-O_5-C_8**	118.50
N_2-H_2	0.820(3)	**C_6-C_7-$0O_5$**	122.95

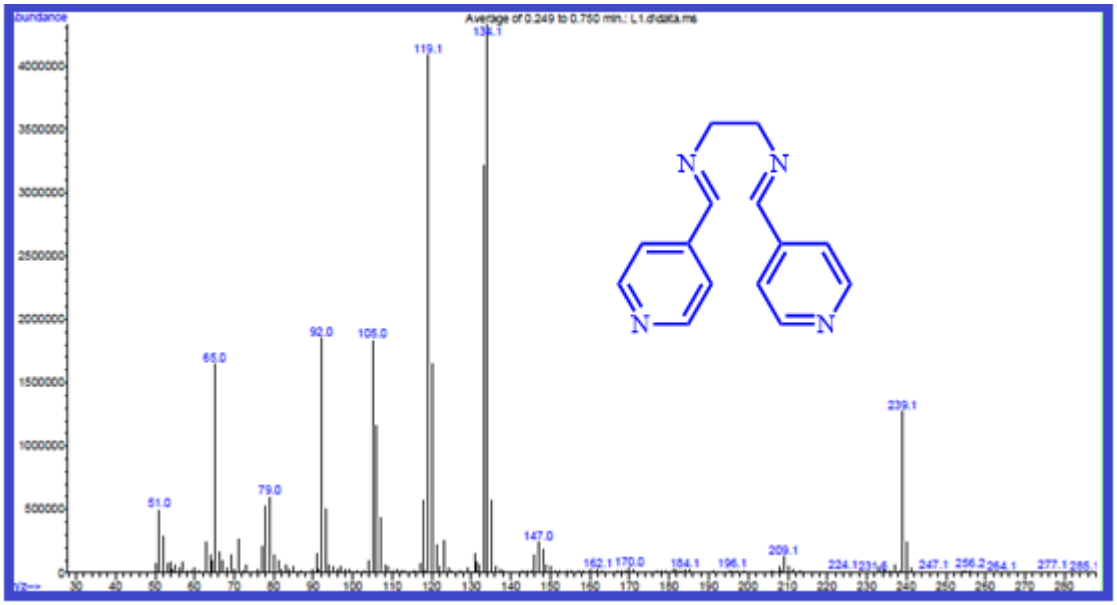

Figure S1. The Mass Spectrum of L.

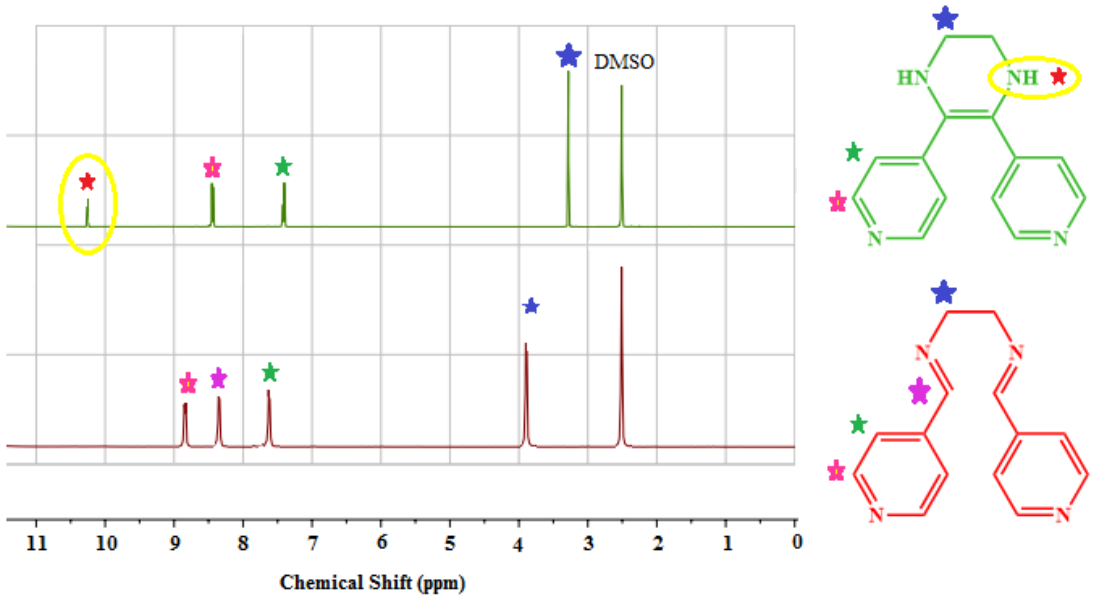

Figure S2. ^{1}H NMR spectrum of L* (top) and L ligand (down) in DMSO as solvent.

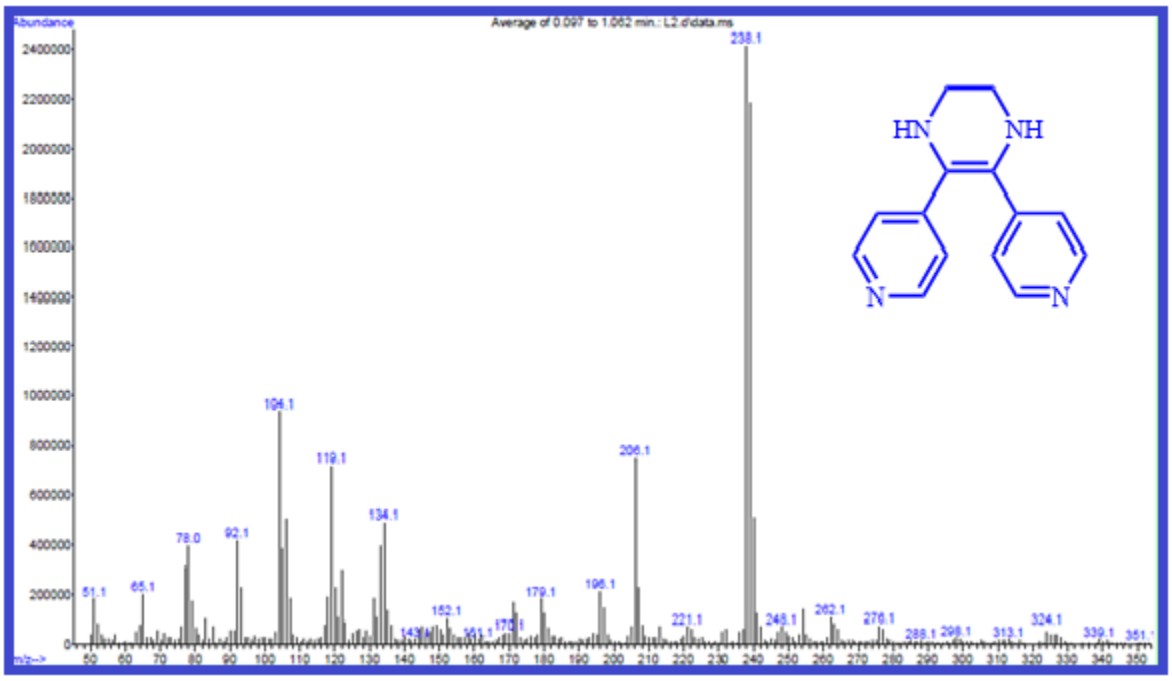

Figure S3. The Mass Spectrum of L*.

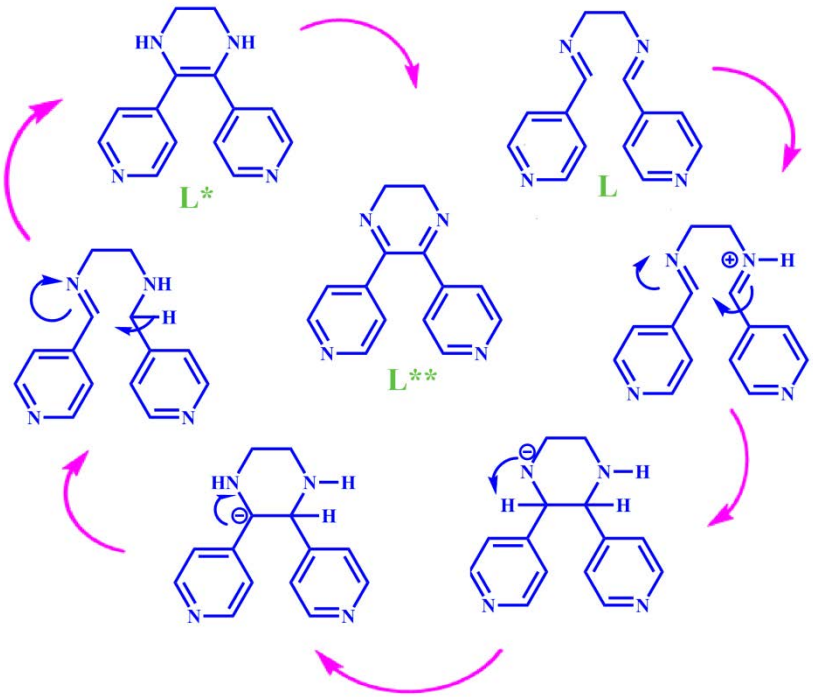

Scheme S1. Proposed mechanism for C=C coupling and cyclization of L to L**.

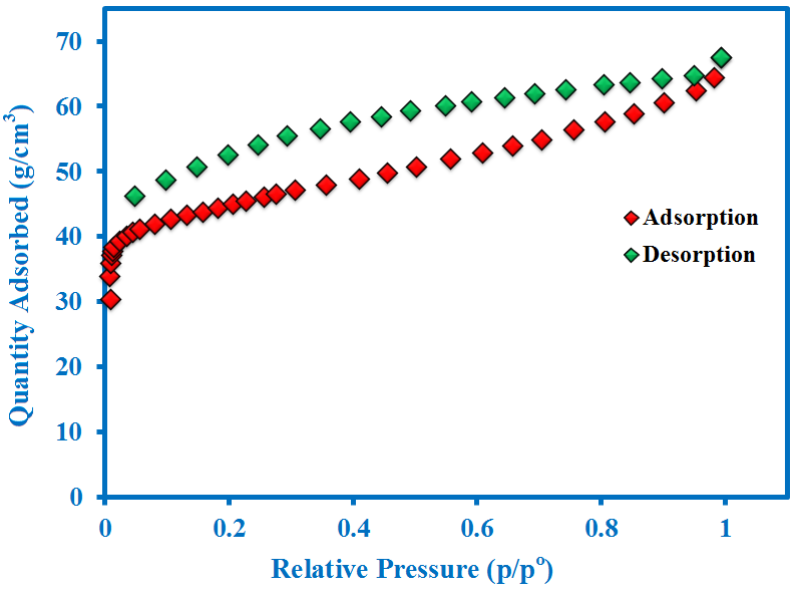

Figure S4. N_2 adsorption-desorption isotherms of TMU-60 after activation.

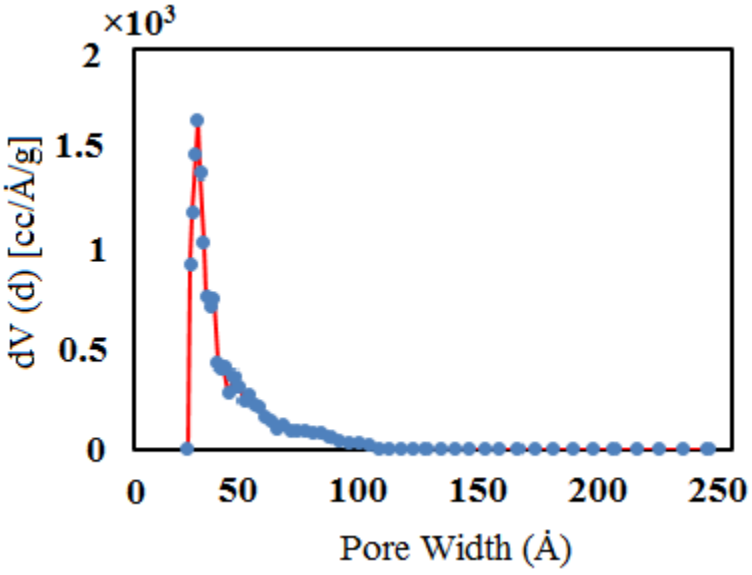

Figure S5. Pore size distribution of TMU-60.

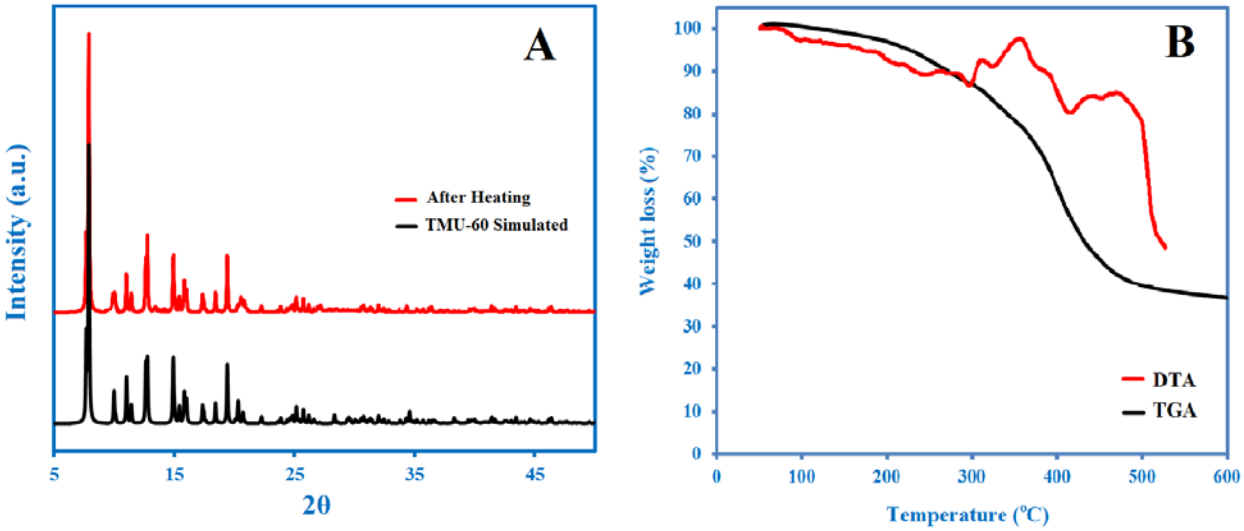

Figure S6. The XRD pattern of TMU-60 after 12h heating in 250˚C (A) and the TGA, DTA curves of the TMU-60.

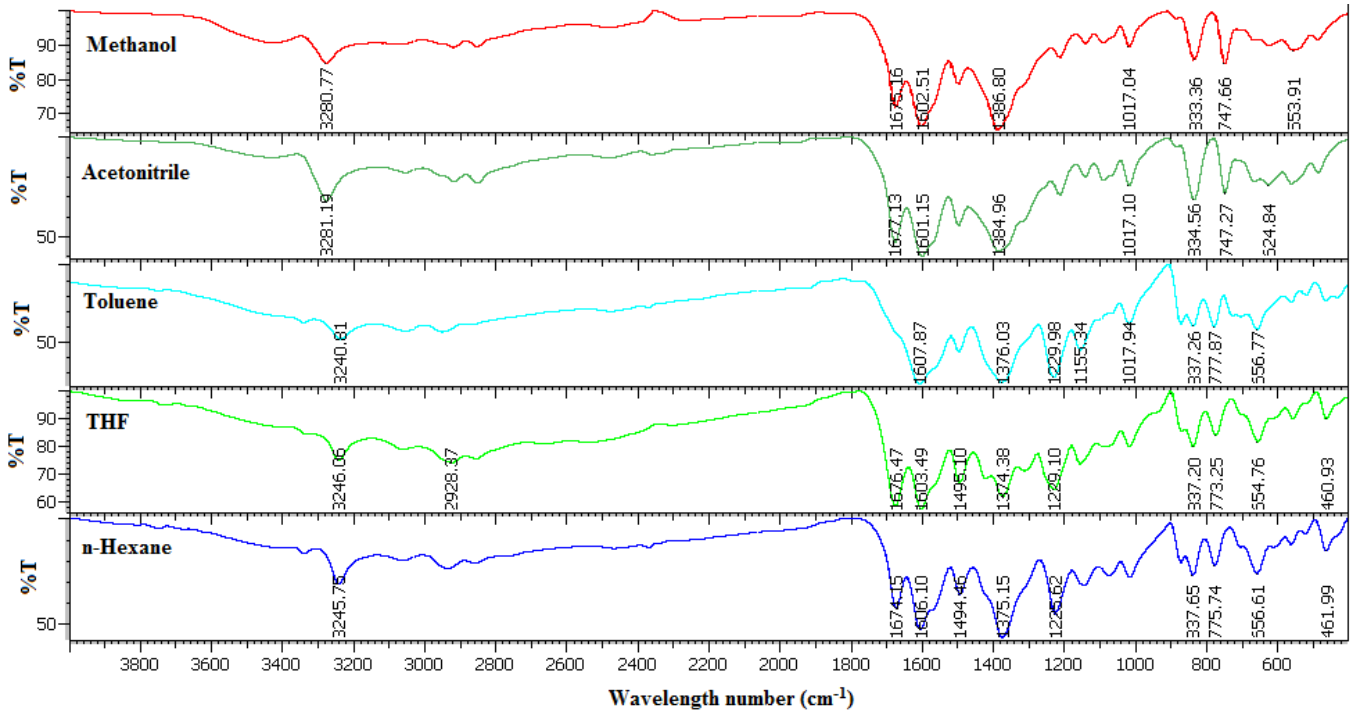

Figure S7. IR spectrum of TMU-60 after 2 hrs immersion in some solvents.

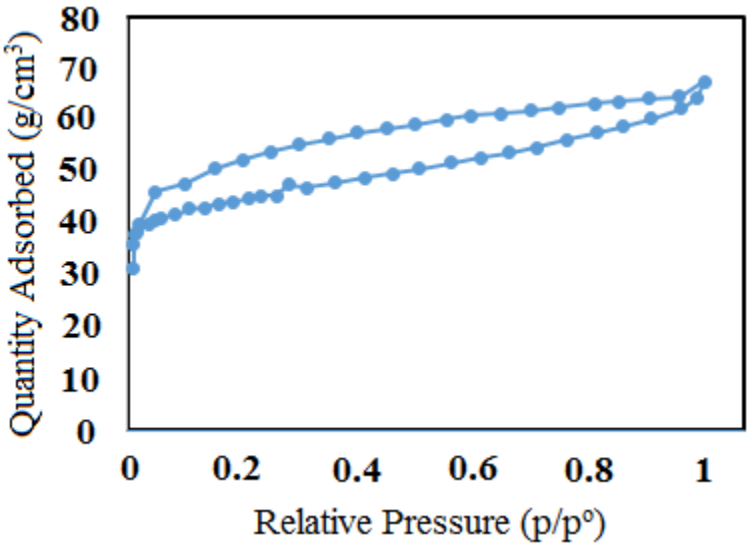

Figure S8. N_2 adsorption-desorption isotherms of O-TMU-60.

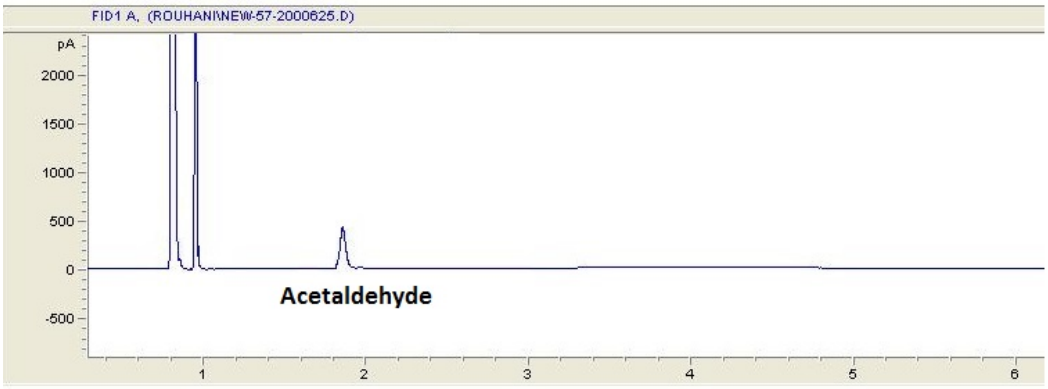

Figure S9. Gas chromatography curves of the acetaldehyde reduction in the presence of TMU-60 and chloroform as solvent.

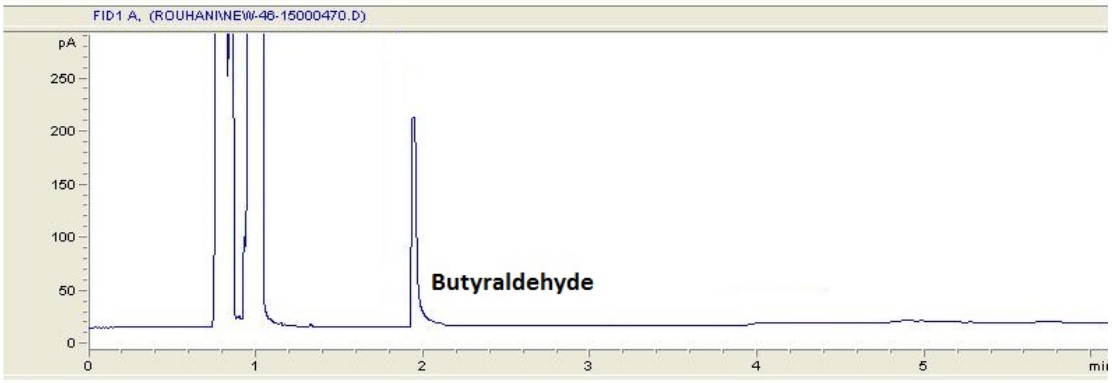

Figure S10. Gas chromatography curves of the butyraldehyde reduction in the presence of TMU-60.

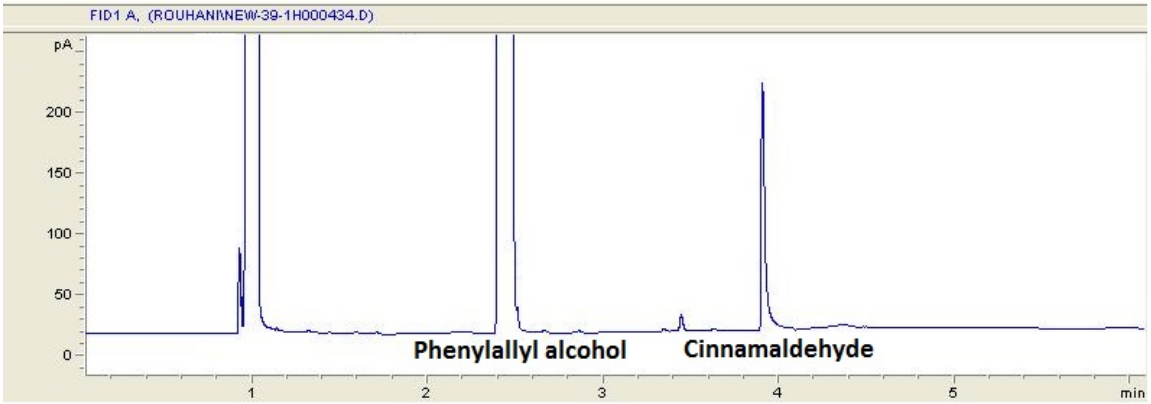

Figure S11. Gas chromatography chart of the cinnemaldehyde reduction in the presence of TMU-60.

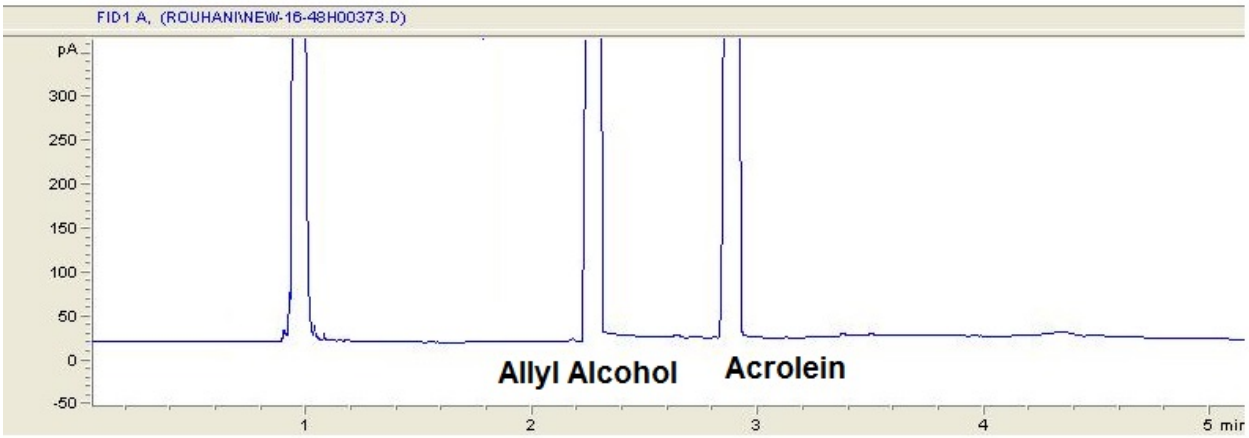

Figure S12. Gas chromatography curves of the acroline reduction in the presence of TMU-60.

Table S2. Optimization of solvent ratio for reduction reaction.

Entry [a]	Reactant	The amount of $CHCl_3$ to DMF (% V/V)	Yield (%)Reduction (Selectivity number)
1	Acetaldehyde	5	60 (90)
2	Acetaldehyde	10	60(90)
3	Acetaldehyde	15	58(82)
4	Acetaldehyde	20	50(80)
5	Acetaldehyde	25	45(80)
6	Acetaldehyde	40	38(73)
7	Acetaldehyde	50	28(70)

[a] the amount of cat:4 mol%, T: 25 ˚C, Time:2h.

Table S3. Comparison of the performance of several catalysts in the aldehyde reduction reaction

Catalyst	Source of Hydrogen	Aldehyde	Time(h)	Temperature	Yield	Selectivity	Ref
Pt NPs	3M Pa H_2	cinnamaldehyde	0.41	R.T	45	18.3	[2]
MIL-101(Cr)	3M Pa H_2	cinnamaldehyde	24	R.T	0	-	[2]
MIL-101(Fe)	3M Pa H_2	cinnamaldehyde	24	R.T	0	-	[2]
MIL-101(Fe)@Pt@MIL-101(Fe)	3M Pa H_2	cinnamaldehyde	10	R.T	45	96	[2]
MIL-101(Cr)@Pt	3M Pa H_2	cinnamaldehyde	0.41	R.T	45	44	[2]
Mn pincer complexe	10 bar H_2	Hydroxymethylfurfural	24	60	90	64	[3]
Ru complex	5M Pa H_2	benzaldehyde	6	100	99	100	[4]
Fe Complex	20 bar H_2	cinnamaldehyde	2	120	97	99	[5]
Fe Complex	30 bar H_2	benzaldehyde	16	40	99	100	[6]
Mg–Al hydrotalcite	MPV method	cinnamaldehyde	5	82	75	92	[7]
TMU-60	solvent	acetaldehyde	2	R.T	63	90	This work

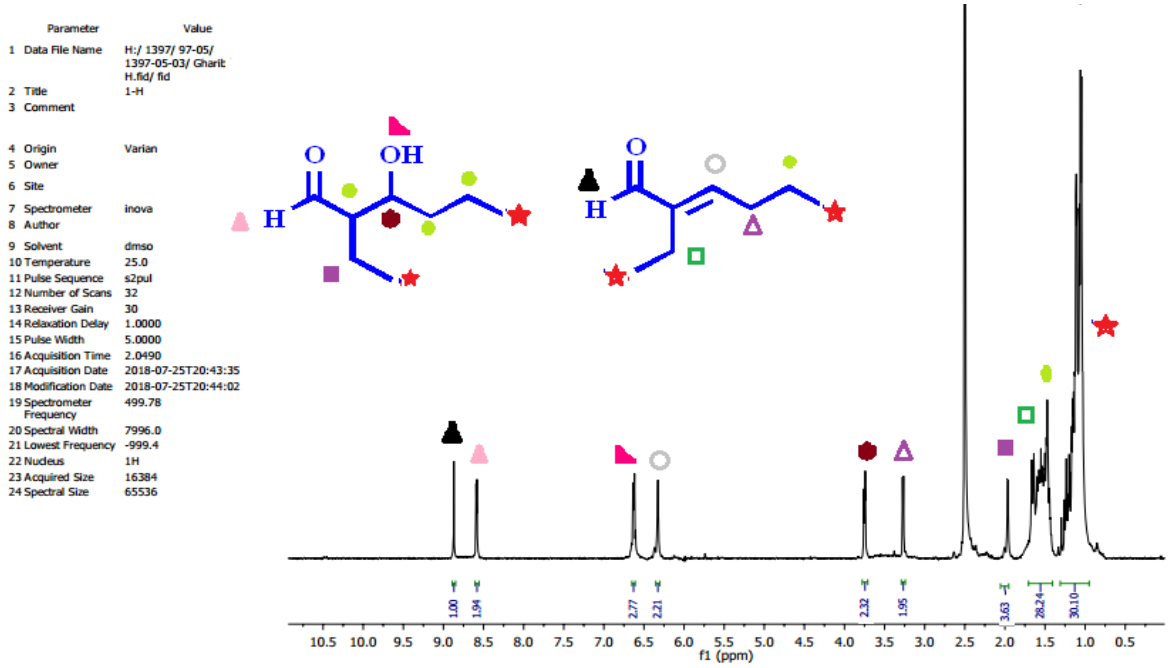

Figure S13. The ^{1}H NMR of the mixture of 2-ethyl-3-hydroxy-hexanal and 2-ethyl-2- hexanal with two to one ratio of condensation of butyraldehyde in the presence of TMU-60 as catalyst.

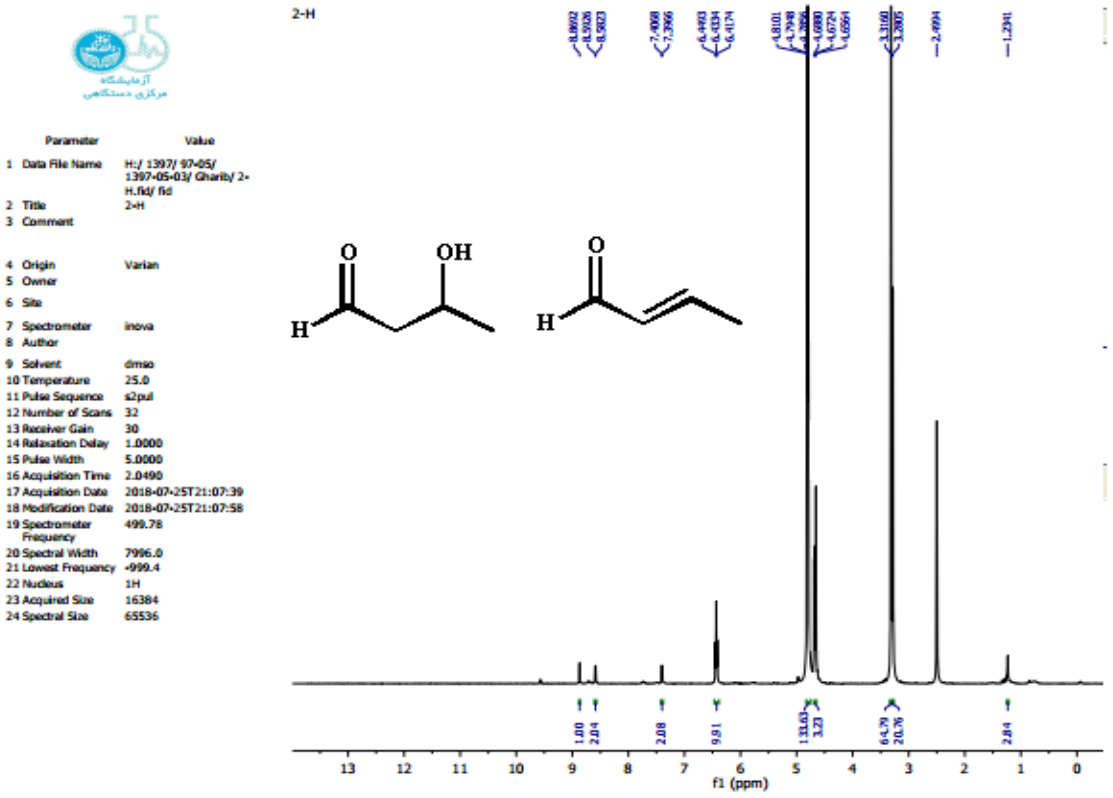

Figure S.14 The ^{1}H NMR spectrum of the crotonaldehyde and 2-hydroxy-butanal resulting of acetaldehyde condensation in the presence of TMU-60.

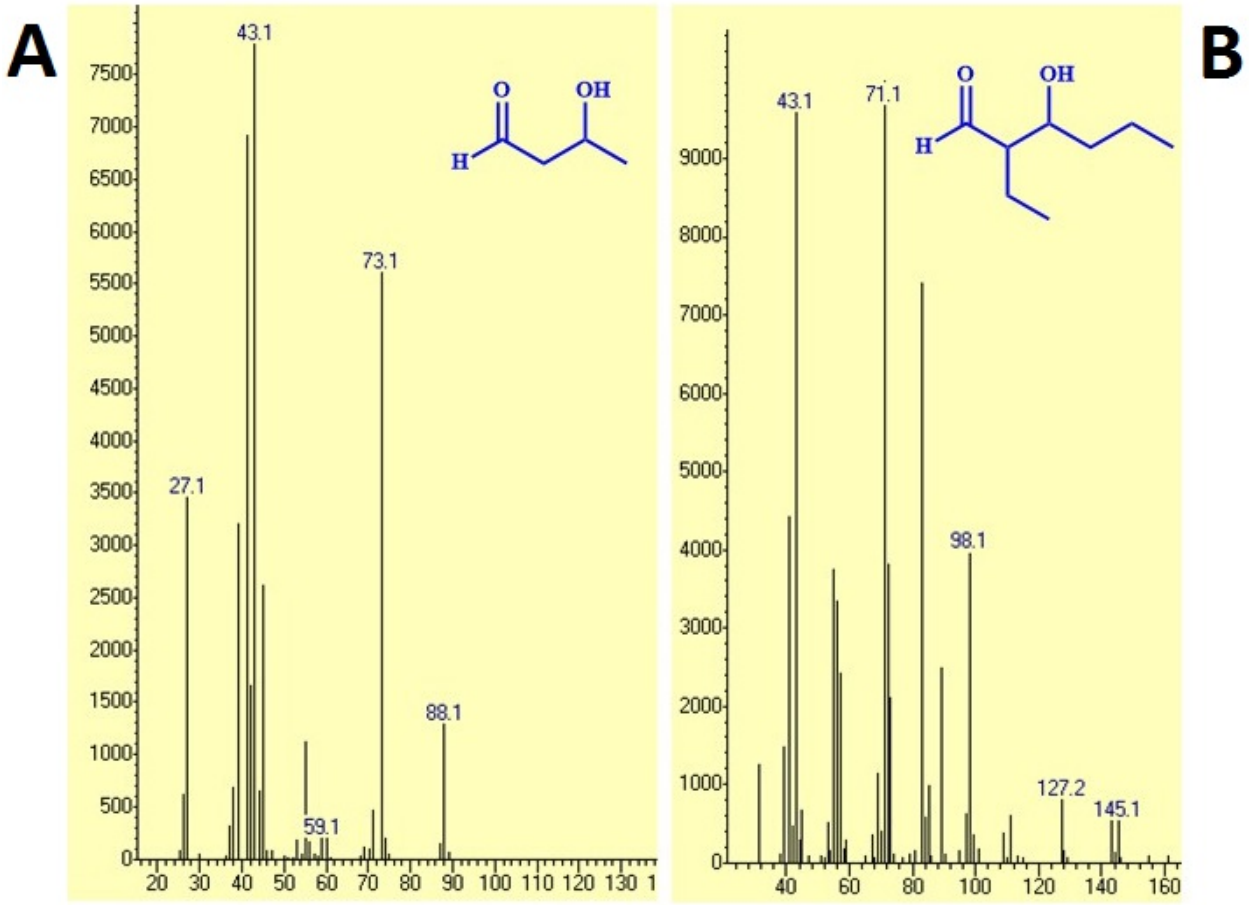

Figure S15. The mass spectrum of condensation product of acetaldehyde (A) and butyraldehyde (B) obtained from GC-Mass injection.

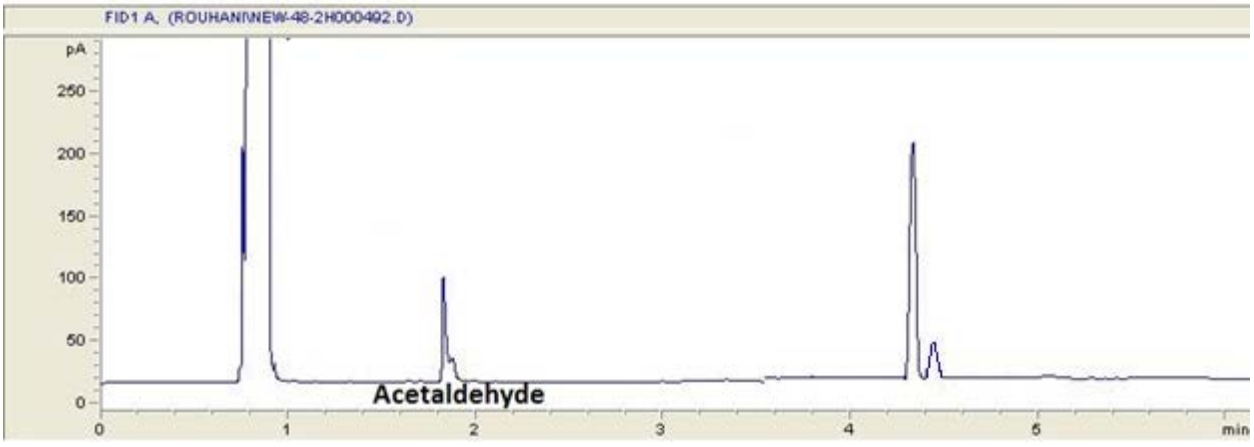

Figure S16. Gas chromatography chart of the acetaldehyde condensation in the presence of TMU-60 as a catalyst.

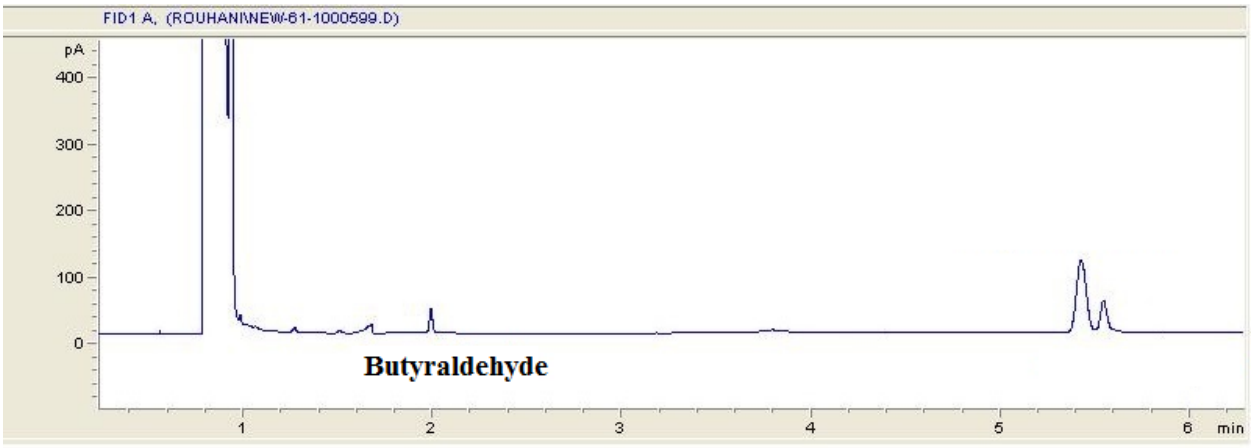

Figure S17. Gas chromatography chart of the butyraldehyde condensation in the presence of TMU-60 as a catalyst.

[1] Patra, Goutam Kumar, and Israel Goldberg. "Coordination polymers of transition metal ions with polydentate imine ligands. Syntheses, materials characterization, and crystal structures of polymeric complexes of copper (I), silver (I) and zinc (II)." Journal of the Chemical Society, Dalton Transactions 6 (2002): 1051-1057.

[2] Zhao, Meiting, et al. "Metal–organic frameworks as selectivity regulators for hydrogenation reactions." Nature 539.7627 (2016): 76.

[3] Elangovan, Saravanakumar, et al. "Selective catalytic hydrogenations of nitriles, ketones, and aldehydes by well-defined manganese pincer complexes." Journal of the American Chemical Society 138.28 (2016): 8809-8814.

[4] Bonomo, Lucia, Laurent Kermorvan, and Philippe Dupau. "Ruthenium-Catalyzed Highly Chemoselective Hydrogenation of Aldehydes." ChemCatChem 7.6 (2015): 907-910.

[5] Wienhoefer, Gerrit, et al. "A Molecularly Defined Iron-Catalyst for the Selective Hydrogenation of α, β-Unsaturated Aldehydes." Chemistry–A European Journal 19.24 (2013): 7701-7707.

[6] Zell, Thomas, Yehoshoa Ben-David, and David Milstein. "Highly efficient, general hydrogenation of aldehydes catalyzed by PNP iron pincer complexes." Catalysis Science & Technology 5.2 (2015): 822-826.

[7] Kumbhar, Pramod S., et al. "Meerwein–Ponndorf–Verley reduction of carbonyl compounds catalysed by Mg–Al hydrotalcite." Chemical Communications 5 (1998): 535-536.